



Characterization of Submicron Organic Particles in Beijing During Summertime: Comparison Between SP-AMS and HR-AMS

Junfeng Wang^{1,2,*}, Jianhuai Ye², Dantong Liu³, Yangzhou Wu³, Jian Zhao⁴, Weiqi Xu⁴,
Conghui Xie⁴, Fuzhen Shen¹, Jie Zhang⁵, Paul E. Ohno², Yiming Qin², Xiuyong Zhao⁶,
Scot T. Martin², Alex K.Y. Lee⁷, Pingqing Fu⁸, Daniel J. Jacob², Qi Zhang⁹, Yele Sun⁴,
Mindong Chen¹ and Xinlei Ge^{1,*}

¹Jiangsu Key Laboratory of Atmospheric Environment Monitoring and Pollution Control, Collaborative Innovation Center of Atmospheric Environment and Equipment Technology, School of Environmental Science and Engineering, Nanjing University of Information Science and Technology, Nanjing, China

²School of Engineering and Applied Sciences, Harvard University, Cambridge, MA, United States

³Department of Atmospheric Sciences, School of Earth Sciences, Zhejiang University, Hangzhou, China

⁴State Key Laboratory of Atmospheric Boundary Layer Physics and Atmospheric Chemistry, Institute of Atmospheric Physics, Chinese Academy of Sciences, Beijing, China

⁵Department of Atmospheric Science, Colorado State University, Fort Collins, CO, United States

⁶State Environmental Protection Key Laboratory of Atmospheric Physical Modeling and Pollution Control, State Power Environmental Protection Research Institute, Nanjing, China

⁷Department of Civil and Environmental Engineering, National University of Singapore, Singapore

⁸Institute of Surface-Earth System Science, Tianjin University, Tianjin, China

⁹Department of Environmental Toxicology, University of California Davis, Davis, CA, United States

*Corresponding author: Xinlei Ge (Email: caxinra@163.com); Junfeng Wang (Email: wangjunfeng@g.harvard.edu).



1 **ABSTRACT**

2 Black carbon (BC) particles in Beijing summer haze play an important role in
3 regional radiation balance and related environmental processes. Understanding the
4 factors that lead to variability in the impacts of BC remains limited. Here, we present
5 observations by a soot-particle aerosol mass spectrometer of BC-containing submicron
6 particulate matter (BC-PM₁) in the summer of 2017 in Beijing, China. These
7 observations were compared to concurrently measured total non-refractory submicron
8 particulate matter (NR-PM₁) by a high-resolution aerosol mass spectrometer (HR-
9 AMS). Distinct properties were observed between NR-PM₁ and BC-PM₁ related to
10 organic aerosol (OA) composition with hydrocarbon-like OA in BC-PM₁ up to two-
11 fold higher than that in NR-PM₁ in fresh vehicle emissions, suggesting that a part of
12 HOA in BC-PM₁ may be overestimated due to the change of the collection efficiency
13 of SP-AMS. Cooking-related OA was only identified in NR-PM₁, whereas aged
14 biomass burning OA (A-BBOA) was a unique factor only identified in BC-PM₁. The
15 A-BBOA was linked to those heavily coated BC, which may lead to enhancement of
16 light absorption ability of BC by a factor of two via the “lensing effect”. More-oxidized
17 oxygenated OA identified in BC-containing particles was found to be slightly different
18 from that observed by HR-AMS, mainly due to the influence of A-BBOA. Overall,
19 these findings highlight that BC in urban Beijing is partly of agricultural fire origin and,
20 a unique biomass burning-related OA associated with BC may be ubiquitous in aged
21 BC-PM₁, and this OA may play a role in affecting air quality and climate that has not
22 previously been fully considered.



23 1. Introduction

24 Black carbon (BC) is an important component of atmospheric aerosol that exerts
25 negative effects on regional radiation balance (Bond et al., 2013) and human health
26 (Janssen, 2012). It absorbs solar radiation, leading to direct atmospheric heating
27 (Ramanathan and Carmichael, 2008). Indirectly, BC-containing particles (BCc) can
28 also serve as cloud condensation nuclei upon mixing with hydrophilic species (e.g.,
29 sulfate), resulting in changes in cloud properties (Wu et al., 2019). Inhalation of BC is
30 associated with adverse health impacts such as respiratory diseases and birth defects
31 (Janssen, 2012).

32 BC particles are released to the atmosphere directly and usually mixed with non-
33 BC materials (e.g., inorganic and organic) from incomplete fuel combustion and open
34 fires (Ramanathan and Carmichael, 2008; Bond et al., 2013; Chen et al., 2013). Non-BC
35 species also can coat onto primary BCc in the atmosphere through condensation and/or
36 coagulation processes (Lee et al., 2017). These atmospheric processes gradually alter
37 the mixing state and the morphology (e.g., from an externally-mixed fractal structure
38 (Buseck et al., 2014) into an internally-mixed “core-shell” structure (China et al., 2015))
39 of BCc. These alterations can enhance the light absorption capacity of the BC core via
40 the “lensing effect” due to the increased light absorption cross-section as a result of the
41 enhanced coating thickness (Saleh et al., 2015; Cappa et al., 2012). Additionally, the
42 chemical constituents of BCc may dynamically change during the aging processes, also
43 lead to changes in the light absorption capacity of the particles (Wang et al., 2019; Wang
44 et al., 2017). Because these physical and chemical processes of both organic and
45 inorganic species inside BCc continuously alter particle properties throughout the
46 lifetime of the particles, great uncertainty remains in quantifying the light absorption
47 ability of BC (Liu et al., 2018; Liu et al., 2019). Understanding the relationship of
48 mixing state and chemical composition to the light absorption properties of BCc, as
49 well as its spatiotemporal distribution, is of importance to accurately evaluate the
50 impacts of BC in regional air quality.

51 Aerodyne high-resolution aerosol mass spectrometry (HR-AMS) (Canagaratna et
52 al., 2007) has been widely applied in field studies to investigate the chemically-resolved
53 composition of non-refractory submicron particulate matter (NR-PM₁, species that
54 vaporize at temperature < 600 °C) (Li et al., 2015; Lee et al., 2013; Sun et al., 2012; Ge
55 et al., 2012b; Ge et al., 2012a; Xu et al., 2019c; Sun et al., 2014). However, the working
56 temperature of the standard HR-AMS tungsten vaporizer (600 °C) is not sufficient to



57 vaporize refractory species such as BC. To overcome this limitation, soot-particle
58 aerosol mass spectrometry (SP-AMS) is developed (Onasch et al., 2012). In addition to
59 the standard tungsten vaporizer, SP-AMS is equipped with a laser vaporizer (with a
60 wavelength of 1064 nm) which selectively heats BC (core), together with the non-BC
61 species mixed with it (Wang et al., 2016). This novel technique makes it possible to
62 compare the compositions of submicron BCc (BC-PM₁) and NR-PM₁, allowing a more
63 accurate assessment of the impacts of BC. However, a question is whether the ion
64 fragments of organic species ionized by the 70eV electron impact of SP-AMS and HR-
65 AMS are the same in terms of different thermal schemes. It has been reported that the
66 mass spectra of NR-PM₁ organic have high m/z 44 (mainly CO₂⁺) signal, while the
67 mass spectra of BC-related organics have high m/z 43 (C₃H₇⁺ and C₂H₃O⁺) signal. The
68 reason for this is the SP-AMS provides vaporization of the BC-PM₁ at lower
69 temperatures compared to the standard tungsten vaporizer of the HR-AMS, resulting in
70 less overall fragmentation and therefore less CO₂⁺ production in the laser, in addition,
71 the lower fragmentation also causes the presence of more ion fragments at m/z > 100
72 amu in the SP-AMS mass spectra compared to that of HR-AMS (Canagaratna et al.,
73 2015b; Massoli et al., 2015). Nevertheless, quantification of BC-PM₁ organic aerosol
74 (OA) factors identified from positive matrix factorization (PMF) has been reported that
75 were not significantly affected by the differences of mass spectra between HR-AMS
76 and SP-AMS (Lee et al., 2017; Massoli et al., 2015).

77 To date, there have only been a few studies that have compared the differences of
78 species in BC-PM₁ and NR-PM₁ (Lee et al., 2017; Collier et al., 2015; Massoli et al.,
79 2015). Lee et al. found that cooking-related organic aerosol (COA) may externally mix
80 with BC in summertime California (Lee et al., 2017). The COA factor was identified in
81 NR-PM₁ organic aerosol (OA), but not in the BC-related OA. Wang et al found that
82 transported biomass burning organic aerosol could be thickly coated on BC in central
83 Tibetan Plateau and significantly enhance the light absorption capacity of BC cores
84 (Wang et al., 2017). Interestingly, the transported biomass burning organic aerosol was
85 not resolved in NR-PM₁ OA particles from concurrent HR-AMS measurements (Xu et
86 al., 2018). These studies suggest that BC-related OA may undergo different
87 atmospheric processes compared to those do not contain BC.

88 Beijing is a megacity known for high particulate matter (PM) concentrations. BC-
89 PM₁ during haze events of summertime Beijing may have distinct sources and
90 properties than other locations in the world. As a part of the UK-China Air Pollution



91 and Human Health (APHH) project summer campaign (Shi et al., 2019), in this study,
92 we focus on the differences of individual species between BC-PM₁ and NR-PM₁
93 regarding their chemical composition, mass loadings, sources, and formation pathways
94 in summertime in urban Beijing. Results from this study provide a better understanding
95 of the formation mechanism of OA particles in Beijing haze and valuable insights in
96 assessing their impacts on air quality.

97

98 **2. Experiments**

99 **2.1. Sampling site and period**

100 The observations were conducted at a rooftop laboratory (8 m above ground level)
101 in the Tower Division of the Institute of Atmospheric Physics (IAP), Chinese Academy
102 of Sciences (CAS) in urban Beijing (39°58'N, 116°22'E), China, from 4 to 29 June,
103 2017. This site has been reported multiple times to be a typical urban observation
104 location (Xie et al., 2019b; Liu et al., 2019; Wang et al., 2019; Qiu et al., 2019; Xu et al.,
105 2019a; Xie et al., 2019a). The site is located around the North 3rd Ring Road of Beijing.
106 A highway is approximately 360 m to the east and a lot of restaurants (e.g., Sichuan
107 style and BBQ) are within 100 m on the north side.

108

109 **2.2. Instrumentation**

110 Two Aerodyne Aerosol Mass Spectrometers (AMS), including a laser-only Soot-
111 Particle AMS (SP-AMS) and a High-Resolution Time of Flight AMS (HR-AMS) were
112 deployed to measure chemical compositions and size distributions of BC-PM₁ and NR-
113 PM₁, respectively. Three types of species were measured during the campaign: NR-
114 PM₁, including BC-free species (Type I) and non-refractory species that mixed with BC
115 (Type II), and BC-PM₁ (BC core and species coated on the core)(Type III). HR-AMS
116 is capable of measuring Type I and Type II, while laser-only SP-AMS can measure
117 Type II and Type III. A shared PM_{2.5} cyclone inlet (Model URG-2000-30ED) with 3
118 Lpm flowrate and a diffusion dryer were used prior to the sampling. The detailed
119 information on the operation of HR-AMS and SP-AMS during the sampling campaign
120 can be found in previous literature (Xie et al., 2019a; Xu et al., 2019d). Details of tuning,
121 calibration, and configurations of the two AMS instruments can be seen in our previous
122 papers (Wang et al., 2019; Xu et al., 2019a; Xu et al., 2019d). Mixing ratios of O₃, and
123 NO₂ (Thermo Fisher Scientific, model 49i and model 42C) were measured in parallel
124 simultaneously. Vertical meteorological parameters, including temperature (*T*) and



125 relative humidity (*RH*), were measured from the IAP 325m meteorological tower.

126

127 **2.3. Data Analysis**

128 AMS data analysis was performed by using Squirrel 1.57 and Pika 1.16I based on
129 Igor Pro 6.37 (WaveMetrics Corp.). The measurement of filtered air was performed for
130 24 hours before the start of the campaign to determine the detection limits of various
131 aerosol species and to adjust the fragmentation table. The relative ionization efficiency
132 (RIE) of BC was calibrated with Regal Black (RB, REGAL 400R pigment black, Cabot
133 Corp.). The average ratio of C_1^+ to C_3^+ ionized from pure BC (RB) was determined to
134 be 0.53, which minimizes the influence of C_1^+ from non-refractory organics. The RIE
135 of BC was determined to be 0.17 based on calibrations performed before, in the middle,
136 and at the end of the campaign. RIEs of NO_3^- , SO_4^{2-} , NH_4^+ were determined to be 1.1,
137 0.82, and 3.82, respectively, and default values of 1.3 and 1.4 for RIEs of Chl and Org
138 were applied, respectively (Canagaratna et al., 2007). Consistent with BC- PM_{10}
139 measurements in previous studies, the RIEs calibration of NO_3^- , SO_4^{2-} , NH_4^+ were
140 performed before the tungsten vaporizer was removed, by assuming those RIEs remain
141 unchanged throughout the campaign (Wang et al., 2017). Polystyrene latex (PSL)
142 spheres (100-700 nm) (Duke Scientific Corp., Palo Alto, CA) were used to calibrate the
143 particle size distribution before the campaign. The collection efficiency (CE) of 0.5
144 were applied for both HR-AMS and SP-AMS in this study. It should be noted that, the
145 BC quantification will not be affected by particle bouncing without the tungsten
146 vaporizer, which could affect the CE in the standard HR-AMS measurements
147 (Canagaratna et al., 2007). However, the CE will be governed by the overlap of particle
148 beam and laser beam (Lee et al., 2017; Massoli et al., 2015; Willis et al., 2014). Both
149 HR-AMS and SP-AMS resolved mass concentrations of NR- PM_{10} and BC were
150 calculated based on V-mode high-resolution fitting. Due to different vaporization
151 schemes between the HR-AMS and SP-AMS, mass spectra from these two instruments
152 even for the same population of aerosols are not entirely the same. Because laser-only
153 SP-AMS generally results in less overall fragmentation, its mass profile may contain
154 more large m/z fragments and less small m/z fragments compared to that from HR-
155 AMS (Massoli et al., 2015). In addition, the elemental ratios of organics reported here,
156 i.e., oxygen-to-carbon and hydrogen-to-carbon ratios (O/C and H/C) were calculated
157 based the “Improved-Ambient (I-A)” method (Canagaratna et al., 2015a).

158 Positive matrix factorization (PMF) (Paatero and Tapper, 1994) was performed on



159 the high-resolution organic mass spectra matrix of both NR-PM₁ and BC-PM₁ (e.g., BC
160 (C_x⁺), and species associated with BC) across m/z 12–120 using PMF Evaluation Tool
161 written in Igor (Ulbrich et al., 2009), following the standard procedure (Zhang et al.,
162 2011). Four types of organic aerosol (OA) from total NR-PM₁ (see our previous
163 paper)(Xu et al., 2019c) and five OA factors from BC-PM₁ were identified. C_x⁺ was
164 involved in the calculation of elemental ratios (e.g, O/C and H/C) of PMF OA factors.
165 All data presented in this paper were averaged hourly and are presented at local time
166 (Beijing Time, UTC+8).

167

168 3. Results and discussion

169 3.1. Overview of observations

170 Figure 1 shows the temporal variations of selected chemical species during the
171 campaign. Information for other variables is provided in the supplementary materials
172 (SM). The two cases labeled in Figure 1 are of interest. Case I (June 8-13) was
173 characterized with high NO₂ concentrations (average 26.7 ± 13.5 ppb, Table S1) and
174 relatively low O₃ concentrations (41.7 ± 30.0 ppb) with NO₂-to-O₃ ratio of 0.64. Case
175 II (June 17-22) was featured by low NO₂ (14.9 ± 5.9 ppb) and high O₃ (84.6 ± 30.6 ppb)
176 concentrations with an NO₂-to-O₃ ratio of 0.18. Unlike winter Beijing haze pollution,
177 RH remained at a relatively low level ($36.5 \pm 15.3\%$), which is not expected to play a
178 significant role in OA formation during the campaign (Figure 1b and Figure S1). In
179 contrast, a strong correlation has been observed between temperature and O₃ ($r^2 = 0.53$).
180 The temperature was higher on average in Case II (29.8 ± 3.8 °C) than in Case I (26.1
181 ± 4.1 °C).

182 The mass concentrations and mass concentration ratios of organic (Org), sulfate
183 (SO₄²⁻) and nitrate (NO₃⁻) in NR-PM₁ (in solid line) and BC-PM₁ (in dotted line) are
184 shown in Figures 1c-e. High correlations were observed between BC-PM₁ and NR-PM₁
185 measurements for SO₄²⁻ ($r^2 = 0.70$) and NO₃⁻ ($r^2 = 0.86$), but not for Org ($r^2 = 0.49$).
186 This result suggests that, BC-PM₁ Org has distinct sources or formation pathways from
187 NR-PM₁ Org. Comparing two cases, the average mass ratios of BC-PM₁ to NR-PM₁ for
188 SO₄²⁻ and NO₃⁻ in Case I (0.24 ± 0.11 and 0.37 ± 0.12) were close to those in Case II
189 (0.19 ± 0.06 and 0.31 ± 0.07). However, ratios of BC-PM₁ to NR-PM₁ for Org were a
190 factor of greater for Case I (0.74 ± 0.32) compare to Case II (0.46 ± 0.13). During the
191 nighttime, this ratio increases to almost unity in Case I. Additionally, BC concentration
192 in Case I (average 2.6 ± 1.6 μg m⁻³) was 1.5 folds higher than in Case II (average $1.7 \pm$



193 0.8 $\mu\text{g m}^{-3}$). The implication is that the organic is mostly associated with BC and likely
194 comprised of freshly emitted compounds in Case I. This is also evident by the moderate
195 correlation between NO_2 and BC-PM₁ Org ($r^2 = 0.42$) in Case I. On the other hand, the
196 lower Org ratio in Case II with higher O_3 concentrations indicates greater oxidation and
197 secondary processes in non-BC particles.

198

199 3.2. Source apportionment of BC-PM₁ OA

200 To further investigate the differences between organics in NR-PM₁ and BC-PM₁,
201 the comparison of PMF OA factors between NR-PM₁ and BC-PM₁ Org is necessary.
202 Four factors were identified from PMF analysis of the NR-PM₁ Org matrix, including
203 hydrocarbon-related OA (HOA), cooking OA (COA), less-oxidized oxygenated OA
204 (LO-OOA), and more-oxidized oxygenated OA (MO-OOA). Details of the NR-PM₁
205 PMF analysis can be found in our previous study (Xu et al., 2019d). Here we only
206 present the PMF results of the SP-AMS measured BC-PM₁ Org. As shown in Figure 2,
207 five factors were resolved by PMF with factors including a HOA, a less oxidized OOA
208 (OOA1), three more-oxidized OOA factors were recombined into one OOA factor
209 (MO-OOA= Aged- biomass burning organic aerosol (A-BBOA) + OOA2 + OOA3).
210 Diagnostic plots of this PMF solution is presented in Figure S2.

211 HOA consists of a series of hydrocarbon fragments (C_xH_y^+) in its mass spectrum
212 (Figure 2f), thus having a low O/C ratio (0.13) but high H/C ratio (1.62). It has a r^2 of
213 0.92 with C_4H_9^+ ($m/z = 57$) and a r^2 of 0.57 with NO_x (Figure 2a), indicative of its
214 sources from vehicle emissions (Xu et al., 2019b). It also correlated tightly with BC (r^2
215 of 0.70) and a series of polycyclic aromatic hydrocarbons (PAHs) ions, e.g., C_9H_7^+ (m/z
216 115, r^2 of 0.63).

217 The second factor has a remarkably high fraction of the biomass burning organic
218 aerosol (BBOA) marker ions of $\text{C}_2\text{H}_4\text{O}_2^+$ ($m/z = 60$) (1.31%) and $\text{C}_3\text{H}_5\text{O}_2^+$ ($m/z = 73$)
219 (1.34%) in its mass spectrum (Figure 2g), much higher than that observed in non-BBOA
220 (e.g., 0.3% at $m/z = 60$) in previous studies (Sun et al., 2016; Xu et al., 2019b; Wang et
221 al., 2017). As expected, the temporal variation of this factor correlated tightly with those
222 of $\text{C}_2\text{H}_4\text{O}_2^+$ and $\text{C}_3\text{H}_5\text{O}_2^+$ (r^2 of 0.71 and 0.72, respectively). In addition, the mass
223 spectrum of this factor is strikingly similar to that of the transported BBOA which was
224 observed at a remote site in the central Tibetan Plateau (Wang et al., 2017), with a r^2 of
225 0.97. Here we categorized the transported BBOA as aged-BBOA (A-BBOA) identified
226 in this study. Similar to the A-BBOA observed in Tibetan Plateau, which has an O/C



227 ratio of 0.51, this factor also has a relatively high O/C ratio of 0.48, greater than that of
228 primary BBOA (O/C of 0.18–0.26)(Wang et al., 2017). These findings support that the
229 second factor may be associated with the oxidation of biomass burning emissions. The
230 temporal variation of ABBOA in the Tibetan Plateau was reported to be highly
231 correlated with the potassium ion fraction (K^+ , r^2 of 0.78), and $K_3SO_4^+$ (r^2 of 0.92).
232 However, the temporal variation of the second factor in this study is only correlated
233 well with that of $K_3SO_4^+$ (r^2 of 0.64) but not K^+ (r^2 of 0.01). The reason for this
234 phenomenon is that the major source of K^+ in remote sites like the Tibetan Plateau was
235 long-distance transport of K_2SO_4 particles, which probably from biomass burning-
236 related K-containing salts interacts with H_2SO_4 (V. Buxton et al., 1999). In contrast,
237 there are multiple primary sources of K^+ in PM_{10} (e.g., diesel-vehicle emissions, and
238 mainly KCl particles) in urban areas (Figure S3). Based on these observations, $K_3SO_4^+$
239 could be defined as an external A-BBOA indicator. Moreover, a previous transmission
240 electron microscopy study also shown that significant agricultural BBOA was mixed
241 with soot and transport from the North China Plain to urban Beijing, meanwhile, K_2SO_4
242 was also identified within those impact single BBOA-soot particles (Li et al., 2010).
243 Hence, this second factor is identified as A-BBOA that was subjected to oxidation
244 during transport to the measurement area as presented in the fire-point map and three-
245 day back trajectories (Figure S4). June should be the month of maximum agricultural-
246 related biomass burning in the North China Plain, although we thought that this burning
247 had been banned in recent years because of air quality concerns (Shen et al., 2019). The
248 implication is that the effectiveness of banning straw burning may be overestimated.

249 The OOA1 factor has an O/C of 0.28 (Figure 2h). Similar to the NR- PM_{10} LO-
250 OOA(Xu et al., 2019c), it is highly correlated with $C_2H_3O^+$ (r^2 of 0.72). The $C_2H_3O^+$
251 ion ($m/z = 43$) is an important component of secondary organic aerosol (SOA)(Collier
252 et al., 2015;Ng et al., 2011) and the diurnal patterns of the OOA1 and $C_2H_3O^+$ both
253 show a great enhancement around noontime (Figure S5), indicating the importance of
254 secondary formation of less oxidized organic aerosol through daytime photochemical
255 activity.

256 The OOA2 factor has an O/C of 0.42 (Figure 2i) and the OOA3 factor has a smaller
257 O/C of 0.32 (Figure 2j). OOA2 correlated strongly with sulfate (r^2 of 0.92; Figure 2d)
258 and OOA3 correlated highly with nitrate (r^2 of 0.97; Figure 2e). These features agree
259 well with the previously observation for low-volatility OOA (sulfate-related OOA) and
260 semi-volatile OOA (nitrate-related OOA) in Tibetan Plateau (Wang et al., 2017).



261 3.3. Comparison of NR-PM₁ and BC-PM₁ OA factors

262 The sum of the above-mentioned BC-PM₁ A-BBOA, OOA₂, and OOA₃ fractions
263 is comparable to the NR-PM₁ MO-OOA factor, based on their high O/C ratios. Figures
264 3a-c are comparisons of the mass loadings of HOA, LO-OOA, and MO-OOA in both
265 NR-PM₁ and BC-PM₁. NR-PM₁ HOA, LO-OOA, and MO-OOA are strongly correlated
266 with their counterpart fractions of BC-PM₁, with r^2 values of 0.68, 0.60, and 0.61,
267 respectively. In Case I, most of the time, the mass loadings of BC-PM₁ HOA and MO-
268 OOA are higher than those in NR-PM₁, while LO-OOA shows the opposite trend. In
269 Case II, the mass loadings of BC-PM₁ HOA are also generally higher than those of NR-
270 PM₁ HOA, however, NR-PM₁ MO-OOA and LO-OOA are almost two folds higher than
271 those of BC-PM₁. Figures 3d-f are comparisons of the fractions of HOA, LO-OOA, and
272 MO-OOA in NR-PM₁ and non-BC material in BC-PM₁ (coatings), respectively. In Case
273 I, the fractions of HOA and MO-OOA internally-mixed with BC are almost two times
274 and four times higher, respectively, than those in NR-PM₁, whereas the two LO-OOA
275 fractions closely track each other. In Case II, two LO-OOA fractions are still overlapped,
276 but compared to Case I, the fraction of HOA in BC-PM₁ coatings is over four times that
277 of NR-PM₁ HOA, and the difference between the two MO-OOA fractions is smaller.

278 As shown in Figure 4, the average of BC-PM₁ HOA fractions (0.27 ± 0.17 and 0.11
279 ± 0.07 , respectively) are higher than those in NR-PM₁ (0.12 ± 0.08 and 0.02 ± 0.02 ,
280 respectively) in both Case I and Case II, indicating that HOA particles is more internally
281 mixed with BC compared to other OA materials. However, the possibility that RIE of
282 OA coating may be lower than the default RIE value should also be considered.

283 The average mass loadings of NR-PM₁ LO-OOA in both Case I and Case II were
284 higher than those of BC-PM₁. However, the fraction of LO-OOA in both NR-PM₁ and
285 BC-PM₁ coatings were very close to each other during the two cases, with an average
286 value of 0.23 ± 0.10 and 0.25 ± 0.12 , respectively, indicating that the probability of LO-
287 OOA condensation onto the two different types of particles is similar.

288 A greater difference between the MO-OOA fractions in NR-PM₁ and BC-PM₁ was
289 observed in Case I than in Case II, and there is more MO-OOA in BC-PM₁ than in NR-
290 PM₁ in Case I. A similar comparison between NR-PM₁ MO-OOA with BC-PM₁ MO-
291 OOA without A-BBOA can be found in SI (Figure S6), which shows closer fractions in
292 both Case I and Case II. Therefore, one possibility which may cause higher MO-OOA
293 fraction in BC-PM₁ than that in NR-PM₁ in Case I is the presence of the BC-PM₁ A-
294 BBOA, which is only identified from the BC-PM₁ OA. More details of the BC-PM₁ A-



295 BBOA are discussed in Section 3.4.

296

297 **3.4. Characteristics of A-BBOA in BC-containing PM₁**

298 Figure 5 shows the high-resolution mass spectra of A-BBOA observed in Nam Co
299 (June 2015) and Beijing (June 2017) by laser-only SP-AMS. A mass spectra very
300 similar to that observed in Beijing was also observed in Nanjing (February 2017)(Wu
301 et al., 2019), with a r^2 of 0.95. The A-BBOA observed in Nam Co (the Tibetan Plateau)
302 was found in the thickest coated and internally-mixed BC-PM₁ (the mass ratio of
303 coatings to BC core (R_{BC}) can reach 14), which enhances the light absorption ability
304 (E_{abs}) of the BC core by a factor of 1.5 to 2.0 via the “lensing effect”.

305 As shown in Figure 6, A-BBOA was associated with those large particles ($D_{va} >$
306 300nm) which were also heavily-coated ($R_{BC} > 9$, Figure 6a and 6c). Because A-BBOA
307 is a moderately aged OA, the OSc was very steady when $R_{BC} > 9$ (Figure 6c). Figure
308 6b presents the fractions of the OA factors (left) and the degree of light absorption
309 enhancement (E_{abs} , estimated by the mass ratios of BC measured by Aethalometer
310 model 33 and SP-AMS), as a function of R_{BC} . Figure 6d shows the temporal variations
311 of the fractions of NR-PM₁ OA and BC-PM₁ OA from 15:00 to 24:00 on June 17, 2017
312 when the highest A-BBOA concentrations were observed. There is a significant
313 enhancement of A-BBOA which may account for up to 60% of the total OA coatings,
314 which could enhance the BC-PM₁ MO-OOA fraction (within the purple frame in the
315 bottom panel of Figure 6d).

316 In this study, A-BBOA was only observed by SP-AMS and was indeed only
317 associated with BC. It is likely that A-BBOA was emitted together with BC when
318 burning biomass fuel, and was oxidized subsequently during the transport. However,
319 we cannot exclude the possibility that A-BBOA can be detected by HR-AMS. For
320 example, it might be included in NR-PM₁ MO-OOA factor. Without separating A-
321 BBOA from other organic species, the source apportionment for HR-AMS may obscure
322 air-quality- and climate-related implications of A-BBOA in the atmosphere, such as the
323 enhancement of aerosol light absorption ability (Figure 6b).



324 **4. Conclusions and implications**

325 Online chemical characteristics of BC and its associated species was for the first
326 time elucidated in urban Beijing in summer, and compared with those of NR-PM₁
327 species. The biggest difference between the two measurements was in the composition
328 of the organic species. In particular, we found BC in urban Beijing in June is partially
329 of agricultural fire origin and, an unique biomass burning-related OA factor (A-BBOA)
330 which was moderately aged, only existed in thickly coated BC-PM₁ ($R_{BC} > 9$), but not
331 NR-PM₁. The unique A-BBOA could make up a significant portion of BC coating
332 material. In addition to Beijing, similar A-BBOA was also identified in other locations,
333 such as central Tibet Plateau (Wang et al., 2017) and Nanjing (Wu et al., 2019),
334 suggesting that it may be ubiquitously present in BC-PM₁ in ambient atmosphere.

335 BBOA species are known to constitute a large portion of light-absorbing organics
336 (brown carbon, BrC). The delay of BBOA oxidation and its longer duration time on BC
337 cores can extend the impacts of BC. Moreover, together with our previous study of BC-
338 associated A-BBOA in Tibet, results presented herein demonstrate that A-BBOA could
339 lead to thick coating on BC cores, meaning a significant “lensing effect” to the
340 enhancement of BC light absorption (Liu et al., 2017). As a key component of BC
341 coating, presence of this factor may also alter the bulk hygroscopicity of BC-PM₁. It
342 could therefore affect its ability as cloud condensation nuclei (CCN)(Wu et al., 2019).
343 Overall, the emission, evolution and transport of such A-BBOA, may influence the
344 atmospheric behaviors and influence the role of BC in the air quality and climate (e.g.,
345 radiative forcing and precipitation). We propose that future laboratory, field, and
346 modeling studies are needed to verify the presence of A-BBOA, and to evaluate the
347 regional environmental impacts of it.

348

Data availability. The data in this study are available from the authors upon request
(caxinra@163.com).

Supplement.

ACKNOWLEDGMENTS

The authors from PRC acknowledge support from the National Natural Science
Foundation of China (21777073) and the National Key Research and Development
Program of China (No. 2018YFC0213802). The authors from Harvard and NUIST



acknowledge additional support through the Harvard-NUIST Joint Laboratory for Air Quality and Climate (JLAQC).

ABBREVIATIONS

BC Black carbon

PM₁ Particulate matter with an aerodynamic diameter smaller than 1 μm

NR-PM₁ non-refractory PM₁

BC-PM₁ BC-containing particles in PM₁

BrC Brown carbon

HR-AMS High-resolution aerosol mass spectrometer (Aerodyne Research Inc.)

SP-AMS Soot-particle aerosol mass spectrometer (Aerodyne Research Inc.)

IE Ionization efficiency

RIE Relative ionization efficiency

HRMS High-resolution mass spectra

PMF Positive matrix factorization

OA Organic aerosol

SOA Secondary organic aerosol O/C Oxygen-to-carbon ratio

H/C Hydrogen-to-carbon ratio

A-BBOA Aged biomass burning organic aerosol

SV-OOA Semi-volatile oxygenated organic aerosol

LV-OOA low-volatility oxygenated organic aerosol

MO-OOA more-oxidized oxygenated organic aerosol

LO-OOA less-oxidized oxygenated organic aerosol

R_{BC} mass ratio of BC coatings to BC

D_{va} Vacuum aerodynamic diameter



REFERENCES

- 349 Bond, T. C., Doherty, S. J., Fahey, D. W., Forster, P. M., Berntsen, T., DeAngelo, B. J., Flanner, M. G.,
350 Ghan, S., Kärcher, B., Koch, D., Kinne, S., Kondo, Y., Quinn, P. K., Sarofim, M. C., Schultz, M. G.,
351 Schulz, M., Venkataraman, C., Zhang, H., Zhang, S., Bellouin, N., Guttikunda, S. K., Hopke, P. K.,
352 Jacobson, M. Z., Kaiser, J. W., Klimont, Z., Lohmann, U., Schwarz, J. P., Shindell, D., Storelvmo, T.,
353 Warren, S. G., and Zender, C. S.: Bounding the role of black carbon in the climate system: A
354 scientific assessment, *J Geophys Res: Atmos*, 118, 5380-5552, 10.1002/jgrd.50171, 2013.
355 Buseck, P. R., Adachi, K., Gelencsér, A., Tompa, É., and Pósfai, M.: Ns-Soot: A Material-Based Term
356 for Strongly Light-Absorbing Carbonaceous Particles, *Aerosol Science and Technology*, 48, 777-
357 788, 10.1080/02786826.2014.919374, 2014.
- 358 Canagaratna, M. R., Jayne, J. T., Jimenez, J. L., Allan, J. D., Alfarra, M. R., Zhang, Q., Onasch, T. B.,
359 Drewnick, F., Coe, H., Middlebrook, A., Delia, A., Williams, L. R., Trimborn, A. M., Northway, M. J.,
360 DeCarlo, P. F., Kolb, C. E., Davidovits, P., and Worsnop, D. R.: Chemical and microphysical
361 characterization of ambient aerosols with the aerodyne aerosol mass spectrometer, *Mass
362 Spectrom Rev*, 26, 185-222, 10.1002/Mas.20115, 2007.
- 363 Canagaratna, M. R., Jimenez, J. L., Kroll, J. H., Chen, Q., Kessler, S. H., Massoli, P., Hildebrandt Ruiz,
364 L., Fortner, E., Williams, L. R., Wilson, K. R., Surratt, J. D., Donahue, N. M., Jayne, J. T., and Worsnop,
365 D. R.: Elemental ratio measurements of organic compounds using aerosol mass spectrometry:
366 characterization, improved calibration, and implications, *Atmos. Chem. Phys.*, 15, 253-272,
367 10.5194/acp-15-253-2015, 2015a.
- 368 Canagaratna, M. R., Massoli, P., Browne, E. C., Franklin, J. P., Wilson, K. R., Onasch, T. B., Kirchstetter,
369 T. W., Fortner, E. C., Kolb, C. E., Jayne, J. T., Kroll, J. H., and Worsnop, D. R.: Chemical Compositions
370 of Black Carbon Particle Cores and Coatings via Soot Particle Aerosol Mass Spectrometry with
371 Photoionization and Electron Ionization, *The Journal of Physical Chemistry A*, 119, 4589-4599,
372 10.1021/jp510711u, 2015b.
- 373 Cappa, C. D., Onasch, T. B., Massoli, P., Worsnop, D. R., Bates, T. S., Cross, E. S., Davidovits, P.,
374 Hakala, J., Hayden, K. L., Jobson, B. T., Kolesar, K. R., Lack, D. A., Lerner, B. M., Li, S.-M., Mellon, D.,
375 Nuaaman, I., Olfert, J. S., Petäjä, T., Quinn, P. K., Song, C., Subramanian, R., Williams, E. J., and Zaveri,
376 R. A.: Radiative absorption enhancements due to the mixing state of atmospheric black carbon,
377 *Science*, 337, 1078-1081, 10.1126/science.1223447, 2012.
- 378 Chen, B., Andersson, A., Lee, M., Kirillova, E. N., Xiao, Q., Kruså, M., Shi, M., Hu, K., Lu, Z., Streets, D.
379 G., Du, K., and Gustafsson, Ö.: Source Forensics of Black Carbon Aerosols from China,
380 *Environmental Science & Technology*, 47, 9102-9108, 10.1021/es401599r, 2013.
- 381 China, S., Scarnato, B., Owen, R. C., Zhang, B., Ampadu, M. T., Kumar, S., Dzepina, K., Dziobak, M.
382 P., Fialho, P., Perlinger, J. A., Hueber, J., Helmig, D., Mazzoleni, L. R., and Mazzoleni, C.: Morphology
383 and mixing state of aged soot particles at a remote marine free troposphere site: Implications for
384 optical properties, *Geophysical Research Letters*, 42, 1243-1250, 10.1002/2014gl062404, 2015.
- 385 Collier, S., Zhou, S., Kuwayama, T., Forestieri, S., Brady, J., Zhang, M., Kleeman, M., Cappa, C.,
386 Bertram, T., and Zhang, Q.: Organic PM Emissions from Vehicles: Composition, O/C Ratio, and
387 Dependence on PM Concentration, *Aerosol Science and Technology*, 49, 86-97,
388 10.1080/02786826.2014.1003364, 2015.
- 389 Ge, X., Zhang, Q., Sun, Y., Ruehl, C. R., and Setyan, A.: Effect of aqueous-phase processing on
390 aerosol chemistry and size distributions in Fresno, California, during wintertime, *Environmental
391 Chemistry*, 9, 221-235, <http://dx.doi.org/10.1071/EN11168>, 2012a.
- 392 Ge, X. L., Setyan, A., Sun, Y., and Zhang, Q.: Primary and secondary organic aerosols in Fresno,
393 California during wintertime: Results from high resolution aerosol mass spectrometry, *J. Geophys.
394 Res.*, 117, D19301, 10.1029/2012jd018026, 2012b.
- 395 Janssen, N. G.-N., Miriam;Lanki,Timo; Salonen,Raimo;Cassee,Flemming; Hoek,Gerard;
396 Fischer,Paul;Brunekreef,Bert;Krzyszczanowski,Michal: Health effects of black carbon, 2012.
- 397 Lee, A. K. Y., Chen, C. L., Liu, J., Price, D. J., Betha, R., Russell, L. M., Zhang, X., and Cappa, C. D.:



- 398 Formation of secondary organic aerosol coating on black carbon particles near vehicular emissions,
399 *Atmos. Chem. Phys.*, 17, 15055–15067, 10.5194/acp-17-15055-2017, 2017.
- 400 Lee, B. P., Li, Y. J., Yu, J. Z., Louie, P. K. K., and Chan, C. K.: Physical and chemical characterization
401 of ambient aerosol by HR-ToF-AMS at a suburban site in Hong Kong during springtime 2011,
402 *Journal of Geophysical Research: Atmospheres*, n/a–n/a, 10.1002/jgrd.50658, 2013.
- 403 Li, W. J., Shao, L. Y., and Buseck, P. R.: Haze types in Beijing and the influence of agricultural biomass
404 burning, *Atmos. Chem. Phys.*, 10, 8119–8130, 10.5194/acp-10-8119-2010, 2010.
- 405 Li, Y. J., Lee, B. P., Su, L., Fung, J. C. H., and Chan, C. K.: Seasonal characteristics of fine particulate
406 matter (PM) based on high-resolution time-of-flight aerosol mass spectrometric (HR-ToF-AMS)
407 measurements at the HKUST Supersite in Hong Kong, *Atmos. Chem. Phys.*, 15, 37–53,
408 10.5194/acp-15-37-2015, 2015.
- 409 Liu, C., Chung, C. E., Yin, Y., and Schnaiter, M.: The absorption Ångström exponent of black carbon:
410 from numerical aspects, *Atmos. Chem. Phys.*, 18, 6259–6273, 10.5194/acp-18-6259-2018, 2018.
- 411 Liu, D., Whitehead, J., Alfara, M. R., Reyes-Villegas, E., Spracklen, Dominick V., Reddington, Carly L.,
412 Kong, S., Williams, Paul I., Ting, Y.-C., Haslett, S., Taylor, Jonathan W., Flynn, Michael J., Morgan,
413 William T., McFiggans, G., Coe, H., and Allan, James D.: Black-carbon absorption enhancement in
414 the atmosphere determined by particle mixing state, *Nature Geoscience*, 10, 184–188,
415 10.1038/ngeo2901, 2017.
- 416 Liu, D., Joshi, R., Wang, J., Yu, C., Allan, J. D., Coe, H., Flynn, M. J., Xie, C., Lee, J., and Squires, F.:
417 Contrasting physical properties of black carbon in urban Beijing between winter and summer,
418 *Atmospheric Chemistry and Physics*, 6749–6769, 2019.
- 419 Massoli, P., Onasch, T. B., Cappa, C. D., Nuamaan, I., Hakala, J., Hayden, K., Li, S.-M., Sueper, D. T.,
420 Bates, T. S., Quinn, P. K., Jayne, J. T., and Worsnop, D. R.: Characterization of black carbon-
421 containing particles from soot particle aerosol mass spectrometer measurements on the R/V
422 Atlantis during CalNex 2010, *Journal of Geophysical Research: Atmospheres*, 120, 2014JD022834,
423 2015.
- 424 Ng, N. L., Canagaratna, M. R., Jimenez, J. L., Chhabra, P. S., Seinfeld, J. H., and Worsnop, D. R.:
425 Changes in organic aerosol composition with aging inferred from aerosol mass spectra, *Atmos.*
426 *Chem. Phys.*, 11, 6465–6474, 10.5194/acp-11-6465-2011, 2011.
- 427 Onasch, T. B., Trimborn, A., Fortner, E. C., Jayne, J. T., Kok, G. L., Williams, L. R., Davidovits, P., and
428 Worsnop, D. R.: Soot Particle Aerosol Mass Spectrometer: Development, Validation, and Initial
429 Application, *Aerosol Science and Technology*, 46, 804–817, 10.1080/02786826.2012.663948, 2012.
- 430 Paatero, P., and Tapper, U.: Positive matrix factorization: A non-negative factor model with optimal
431 utilization of error estimates of data values, *Environmetrics*, 5, 111–126, 10.1002/env.3170050203,
432 1994.
- 433 Qiu, Y., Xie, Q., Wang, J., Xu, W., Li, L., Wang, Q., Zhao, J., Chen, Y., Chen, Y., Wu, Y., Du, W., Zhou,
434 W., Lee, J., Zhao, C., Ge, X., Fu, P., Wang, Z., Worsnop, D. R., and Sun, Y.: Vertical Characterization
435 and Source Apportionment of Water-Soluble Organic Aerosol with High-resolution Aerosol Mass
436 Spectrometry in Beijing, China, *ACS Earth and Space Chemistry*, 3, 273–284,
437 10.1021/acsearthspacechem.8b00155, 2019.
- 438 Ramanathan, V., and Carmichael, G.: Global and regional climate changes due to black carbon,
439 *Nature Geosci.*, 1, 221–227, 2008.
- 440 Saleh, R., Marks, M., Heo, J., Adams, P. J., Donahue, N. M., and Robinson, A. L.: Contribution of
441 brown carbon and lensing to the direct radiative effect of carbonaceous aerosols from biomass
442 and biofuel burning emissions, *Journal of Geophysical Research: Atmospheres*, 120, 2085–
443 210,296, 10.1002/2015jd023697, 2015.
- 444 Shen, L., Jacob, D. J., Zhu, L., Zhang, Q., Zheng, B., Sulprizio, M. P., Li, K., De Smedt, I., González
445 Abad, G., Cao, H., Fu, T.-M., and Liao, H.: The 2005–2016 Trends of Formaldehyde Columns Over
446 China Observed by Satellites: Increasing Anthropogenic Emissions of Volatile Organic Compounds
447 and Decreasing Agricultural Fire Emissions, *Geophysical Research Letters*, 46, 4468–4475,
448 10.1029/2019gl082172, 2019.



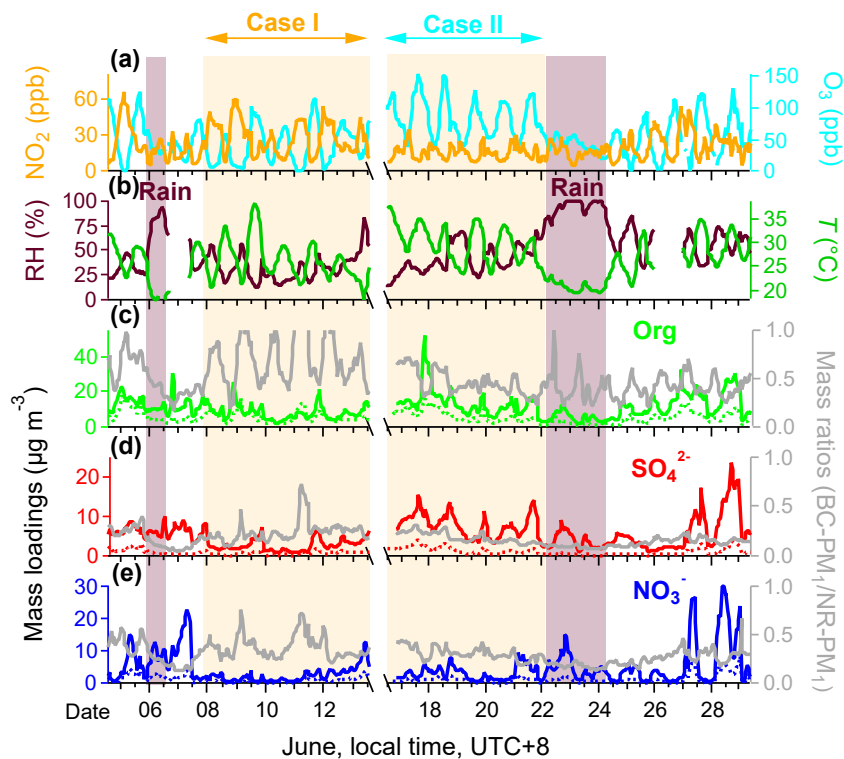
- 449 Shi, Z., Vu, T., Kotthaus, S., Harrison, R. M., Grimmond, S., Yue, S., Zhu, T., Lee, J., Han, Y., Demuzere,
450 M., Dunmore, R. E., Ren, L., Liu, D., Wang, Y., Wild, O., Allan, J., Acton, W. J., Barlow, J., Barratt, B.,
451 Beddows, D., Bloss, W. J., Calzolari, G., Carruthers, D., Carslaw, D. C., Chan, Q., Chatzidiakou, L.,
452 Chen, Y., Crilley, L., Coe, H., Dai, T., Doherty, R., Duan, F., Fu, P., Ge, B., Ge, M., Guan, D., Hamilton,
453 J. F., He, K., Heal, M., Heard, D., Hewitt, C. N., Hollaway, M., Hu, M., Ji, D., Jiang, X., Jones, R., Kalberer,
454 M., Kelly, F. J., Kramer, L., Langford, B., Lin, C., Lewis, A. C., Li, J., Li, W., Liu, H., Liu, J., Loh, M., Lu, K.,
455 Lucarelli, F., Mann, G., McFiggans, G., Miller, M. R., Mills, G., Monk, P., Nemitz, E., O'Connor, F.,
456 Ouyang, B., Palmer, P. I., Percival, C., Popoola, O., Reeves, C., Rickard, A. R., Shao, L., Shi, G.,
457 Spracklen, D., Stevenson, D., Sun, Y., Sun, Z., Tao, S., Tong, S., Wang, Q., Wang, W., Wang, X., Wang,
458 X., Wang, Z., Wei, L., Whalley, L., Wu, X., Wu, Z., Xie, P., Yang, F., Zhang, Q., Zhang, Y., Zhang, Y.,
459 and Zheng, M.: Introduction to the special issue "In-depth study of air pollution sources and
460 processes within Beijing and its surrounding region (APHH-Beijing)", *Atmos. Chem. Phys.*, 19,
461 7519-7546, 10.5194/acp-19-7519-2019, 2019.
- 462 Sun, Y., Jiang, Q., Wang, Z., Fu, P., Li, J., Yang, T., and Yin, Y.: Investigation of the Sources and
463 Evolution Processes of Severe Haze Pollution in Beijing in January 2013, *Journal of Geophysical
464 Research: Atmospheres*, 2014JD021641, 10.1002/2014JD021641, 2014.
- 465 Sun, Y., Jiang, Q., Xu, Y., Ma, Y., Zhang, Y., Liu, X., Li, W., Wang, F., Li, J., Wang, P., and Li, Z.: Aerosol
466 characterization over the North China Plain: Haze life cycle and biomass burning impacts in
467 summer, *Journal of Geophysical Research: Atmospheres*, 121, 2508-2521, 10.1002/2015jd024261,
468 2016.
- 469 Sun, Y. L., Zhang, Q., Schwab, J. J., Chen, W. N., Bae, M. S., Hung, H. M., Lin, Y. C., Ng, N. L., Jayne,
470 J., Massoli, P., Williams, L. R., and Demerjian, K. L.: Characterization of near-highway submicron
471 aerosols in New York City with a high-resolution aerosol mass spectrometer, *Atmos. Chem. Phys.*,
472 12, 2215-2227, 10.5194/acp-12-2215-2012, 2012.
- 473 Ulbrich, I. M., Canagaratna, M. R., Zhang, Q., Worsnop, D. R., and Jimenez, J. L.: Interpretation of
474 organic components from Positive Matrix Factorization of aerosol mass spectrometric data, *Atmos.
475 Chem. Phys.*, 9, 2891-2918, 10.5194/acp-9-2891-2009, 2009.
- 476 V. Buxton, G., Bydder, M., and Arthur Salmon, G.: The reactivity of chlorine atoms in aqueous
477 solution Part II. The equilibrium $\text{SO}_4^- + \text{Cl}^- \rightleftharpoons \text{ClSO}_3^- + \text{SO}_4^{2-}$, *Physical Chemistry Chemical Physics*, 1,
478 269-273, 10.1039/A807808D, 1999.
- 479 Wang, J., Onasch, T. B., Ge, X., Collier, S., Zhang, Q., Sun, Y., Yu, H., Chen, M., Prévôt, A. S., and
480 Worsnop, D. R.: Observation of fullerene soot in eastern China, *Environmental Science &
481 Technology Letters*, 3, 121-126, 2016.
- 482 Wang, J., Zhang, Q., Chen, M., Collier, S., Zhou, S., Ge, X., Xu, J., Shi, J., Xie, C., and Hu, J.: First
483 chemical characterization of refractory black carbon aerosols and associated coatings over the
484 Tibetan Plateau (4730 m asl), *Environmental science & technology*, 51, 14072-14082, 2017.
- 485 Wang, J., Liu, D., Ge, X., Wu, Y., Shen, F., Chen, M., Zhao, J., Xie, C., Wang, Q., and Xu, W.:
486 Characterization of black carbon-containing fine particles in Beijing during wintertime,
487 *Atmospheric Chemistry and Physics*, 19, 447-458, 2019.
- 488 Willis, M. D., Lee, A. K. Y., Onasch, T. B., Fortner, E. C., Williams, L. R., Lambe, A. T., Worsnop, D. R.,
489 and Abbatt, J. P. D.: Collection efficiency of the soot-particle aerosol mass spectrometer (SP-AMS)
490 for internally mixed particulate black carbon, *Atmos. Meas. Tech.*, 7, 4507-4516, 10.5194/amt-7-
491 4507-2014, 2014.
- 492 Wu, Y., Liu, D., Wang, J., Shen, F., Chen, Y., Cui, S., Ge, S., Wu, Y., Chen, M., and Ge, X.:
493 Characterization of Size-Resolved Hygroscopicity of Black Carbon-Containing Particle in Urban
494 Environment, *Environmental science & technology*, 53, 14212-14221, 2019.
- 495 Xie, C., Xu, W., Wang, J., Liu, D., Ge, X., Zhang, Q., Wang, Q., Du, W., Zhao, J., Zhou, W., Li, J., Fu, P.,
496 Wang, Z., Worsnop, D., and Sun, Y.: Light absorption enhancement of black carbon in urban Beijing
497 in summer, *Atmos Environ*, 213, 499-504, <https://doi.org/10.1016/j.atmosenv.2019.06.041>, 2019a.
- 498 Xie, C., Xu, W., Wang, J., Wang, Q., Liu, D., Tang, G., Chen, P., Du, W., Zhao, J., and Zhang, Y.:
499 Vertical characterization of aerosol optical properties and brown carbon in winter in urban Beijing,



- 500 China, *Atmospheric Chemistry and Physics*, 19, 165-179, 2019b.
501 Xu, J., Zhang, Q., Shi, J., Ge, X., Xie, C., Wang, J., Kang, S., Zhang, R., and Wang, Y.: Chemical
502 characteristics of submicron particles at the central Tibetan Plateau: insights from aerosol mass
503 spectrometry, *Atmospheric Chemistry and Physics*, 18, 2018.
504 Xu, W., Sun, Y., Wang, Q., Zhao, J., Wang, J., Ge, X., Xie, C., Zhou, W., Du, W., and Li, J.: Changes in
505 aerosol chemistry from 2014 to 2016 in winter in Beijing: Insights from high-resolution aerosol
506 mass spectrometry, *Journal of Geophysical Research: Atmospheres*, 124, 1132-1147, 2019a.
507 Xu, W., Sun, Y., Wang, Q., Zhao, J., Wang, J., Ge, X., Xie, C., Zhou, W., Du, W., and Li, J.: Changes in
508 aerosol chemistry from 2014 to 2016 in winter in Beijing: Insights from high-resolution aerosol
509 mass spectrometry, *J Geophys Res: Atmos*, 124, 1132-1147, 2019b.
510 Xu, W., Xie, C., Karnezi, E., Zhang, Q., Wang, J., Pandis, S. N., Ge, X., Zhang, J., An, J., and Wang, Q.:
511 Summertime aerosol volatility measurements in Beijing, China, *Atmos Chem Phys*, 19, 10205-
512 10216, 2019c.
513 Xu, W., Xie, C., Karnezi, E., Zhang, Q., Wang, J., Pandis, S. N., Ge, X., Zhang, J., An, J., Wang, Q.,
514 Zhao, J., Du, W., Qiu, Y., Zhou, W., He, Y., Li, Y., Li, J., Fu, P., Wang, Z., Worsnop, D. R., and Sun, Y.:
515 Summertime aerosol volatility measurements in Beijing, China, *Atmos. Chem. Phys.*, 19, 10205-
516 10216, 10.5194/acp-19-10205-2019, 2019d.
517 Zhang, Q., Jimenez, J., Canagaratna, M., Ulbrich, I., Ng, N., Worsnop, D., and Sun, Y.: Understanding
518 atmospheric organic aerosols via factor analysis of aerosol mass spectrometry: a review, *Analytical
519 and Bioanalytical Chemistry*, 401, 3045-3067, 10.1007/s00216-011-5355-y, 2011.

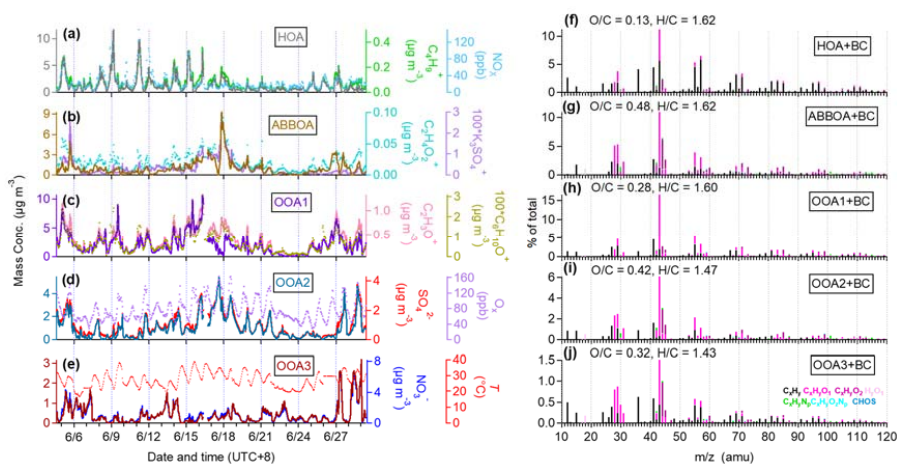


520



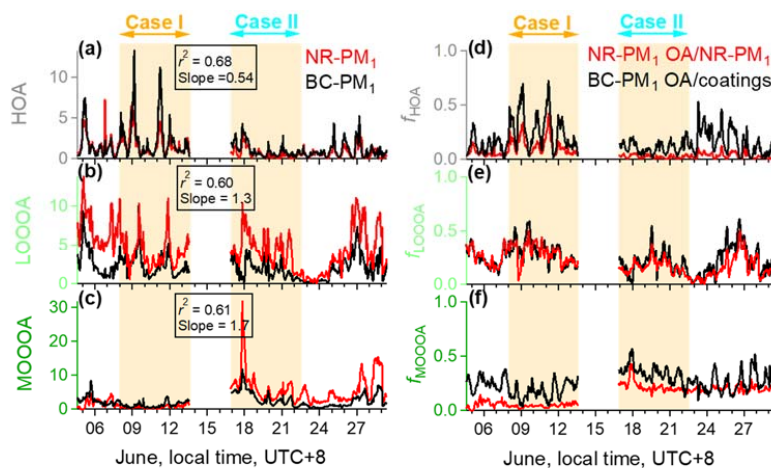
521

522 **Figure 1.** Temporal variations of selected chemical species measured in Beijing on June 4-29, 2017.
523 (a) mixing ratios of nitrogen dioxide (NO_2) and ozone (O_3); (b) 15-m relative humidity (RH) and
524 temperature (T); (c-e) on the left are the mass loadings of organic (Org), sulfate (SO_4^{2-}) and nitrate
525 (NO_3^-) measured by HR-AMS and SP-AMS, and on the right are mass ratios of individual BC- PM_{10}
526 species to NR- PM_{10} species (e.g., BC- PM_{10} Org to NR- PM_{10} Org). The NR- PM_{10} species measured by
527 HR-AMS is in solid line, and the BC- PM_{10} species measured by SP-AMS is in the dotted line. The
528 shaded areas are raining periods. The observation period is divided into two cases according to the
529 mixing ratio of nitrogen NO_2 , Case I and Case II, which represent high NO_2 and low NO_2 mixing
530 ratios, respectively.



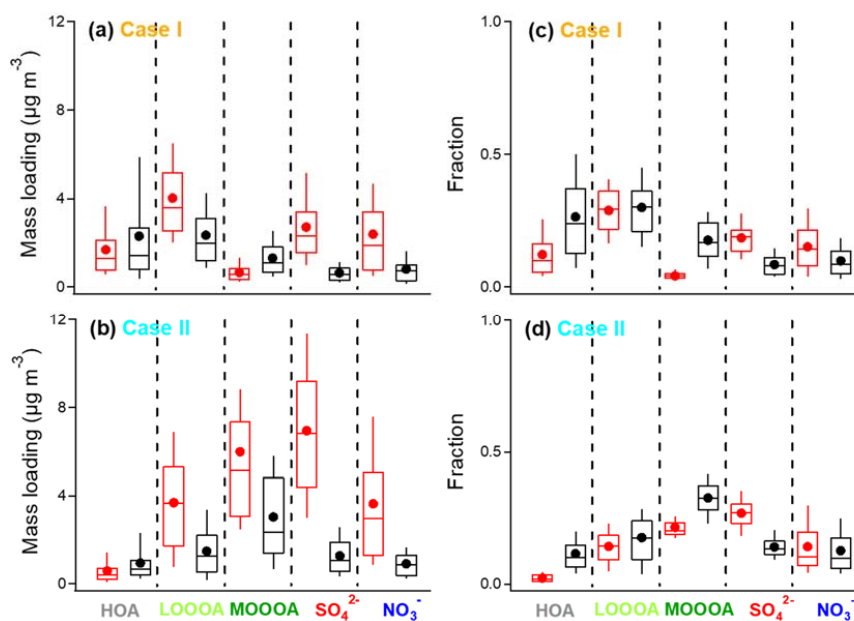
531

532 **Figure 2.** Temporal variations (left panels), high-resolution mass spectra (right panels) of five OA
533 factors in summer 2017: (a) and (f) HOA, (b) and (g) A-BBOA, (c) and (h) OOA1 (LO-OOA), (d)
534 and (i) OOA2, and (e) and (j) OOA3. Also shown in the left panels are the time series of other tracers,
535 including $C_4H_9^+$, NO_x , $C_2H_4O_2^+$, $K_3SO_4^+$, $C_6H_{10}O^+$, $C_2H_3O^+$, SO_4^{2-} and NO_3^- .

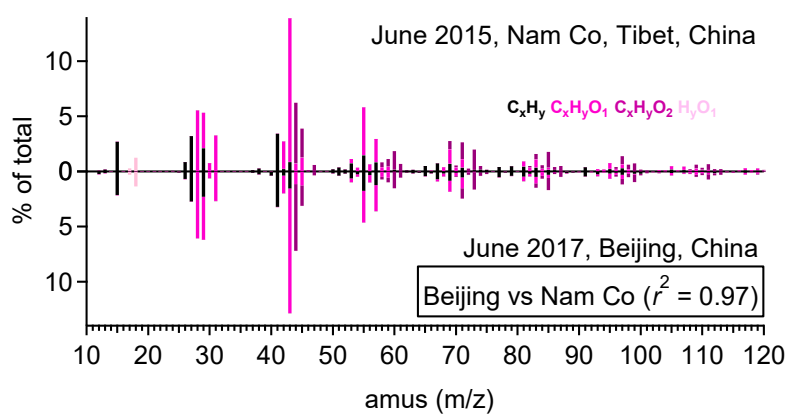


536

537 **Figure 3.** Temporal variations of NR-PM₁ and BC-PM₁ (a-c) HOA, LO-OOA, and MO-OOA (left
538 panels) and (d-e) their fractions. NR-PM₁ OA factors are in red, and the BC-PM₁ OA factors are in
539 black. Here BC-PM₁ MO-OOA is the sum of A-BBOA, OOA2 (sulfate-related OOA), and OOA3
540 (nitrate-related OOA).



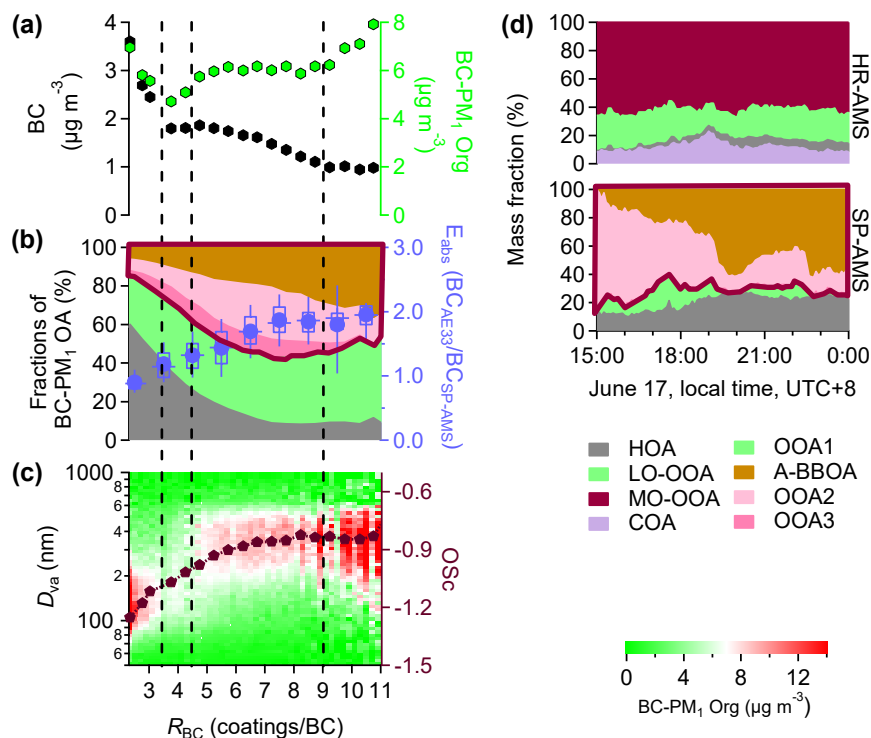
541
542 **Figure 4.** Box plots of mass loadings and fractions of five selected species (HOA, LO-OOA, MO-
543 OOA, SO_4^{2-} , and NO_3^-) in Case I and Case II. The bounds of boxes represent quartiles, the whiskers
544 indicate the 90th and 10th percentiles, and the lines and dots inside the boxes are median and mean
545 values. NR-PM₁ OA factors are in red, and the BC-PM₁ OA factors are in black.



546

547 **Figure 5** Comparison between the high-resolution mass spectra of A-BBOA obtained in Nam Co

548 (June 2015) and Beijing (June 2017).



549
 550 **Figure 6.** (a-c) the mass loadings of BC, BC-PM₁ Org, fractions of BC-PM₁ OA factors, E_{abs} , the
 551 oxidation state ($\text{OSc} = 2*(\text{O}/\text{C}) - (\text{H}/\text{C})$) of BC-PM₁ Org, and the size distribution of BC-PM₁ Org
 552 as a function of coating thickness (R_{BC}). (d) temporal variations of OA fractions of NR-PM₁ and
 553 BC-PM₁ from 15:00 to 24:00 on June 17, 2017.
 554